

Quantifying the effects of peripheral substituents on the spin-lattice relaxation of a vanadyl molecular quantum bit

Stefan H. Lohaus^a, Nathanael P. Kazmierczak^a, Kaitlin M. Luedecke^a, Benjamin Marx^b, Victor N. Nemykin^{b,o}, and Ryan G. Hadt^{a,o,*}

^aDivision of Chemistry and Chemical Engineering, Arthur Amos Noyes Laboratory of Chemical Physics, California Institute of Technology, Pasadena, CA 91125, USA

Received 29 April 2024 Accepted 10 June 2024

ICPP-13 Award paper

ABSTRACT: Electron spin superpositions represent a critical component of emergent quantum technologies in computation, sensing, encryption, and communication. However, spin relaxation (T_1) and decoherence (T_m) represent major obstacles to the implementation of molecular quantum bits (qubits). Synthetic strategies have made substantial progress in enhancing spin coherence times by minimizing contributions from surrounding electron and nuclear spins. For room-temperature operation, however, the lifetime of spin coherence becomes limited by coupling with vibrational modes of the lattice. Using pulse electron paramagnetic resonance (EPR) spectroscopy, we measure the spin-lattice relaxation of a vanadyl tetrapyrazinoporphyrazine complex appended with eight peripheral 2,6-diisopropylphenol groups (VOPyzPz-DIPP) and compare it to the relaxation of the archetypical vanadyl phthalocyanine molecular qubit (VOPc). The added peripheral groups lead to distinctly different spin relaxation behavior. While similar relaxation times are observed at low temperatures and ambient conditions, significant changes are observed for the orientation dependence of T_1 at 100 K, as well as the temperature dependence of T_1 over the intermediate temperature range spanning \sim 10–150 K. These results can be tentatively interpreted as arising from loosened spin-phonon coupling selection rules and a greater number of accessible acoustic and optical modes contributing to the spin relaxation behavior of VOPyzPz-DIPP relative to VOPc.

KEYWORDS: Molecular qubits, Vanadyl phthalocyanine, Spin-lattice relaxation time, Spin-phonon coupling, Pulse EPR.

INTRODUCTION

The development of quantum computation and sensing is limited by the coherence times of current quantum bits (qubits) of information. In contrast to a $|0\rangle$ or $|1\rangle$ binary bit, a qubit can carry more information due to its ability to form superpositions of such states. For a successful quantum computation, the coherence time of the

superposition, or phase memory time, $T_{\rm m}$, must be at least 10^4 times longer than that of an individual quantum operation [1, 2]; in electron paramagnetic resonance (EPR), the operation time corresponds to a microwave pulse of ~8 ns. Electron spins are attractive qubit candidates, as they can take on superpositions of their M_S sublevels in applied magnetic fields and can be manipulated and sensed by established methods. $S=\frac{1}{2}$ Cu(II) and vanadyl phthalocyanines (CuPc/VOPc) are among the most highly studied molecular qubits; VOPc also represents one of the rare transition metal systems exhibiting measurable spin coherence up to room temperature [3–6].

^bDepartment of Chemistry, University of Tennessee – Knoxville, Knoxville, TN 37996, USA

SPP full member in good standing.

^{*}Correspondence to: Ryan G. Hadt, e-mail: rghadt@caltech.edu.

Phthalocyanines can also be deposited onto surfaces for device fabrication [7] and integrated with solid-state systems into hybrid quantum architectures [8, 9]. However, as temperature increases, vibrational modes of the molecules and phonons of the crystal become populated and interact with spins. This spin-lattice relaxation limits the coherence of the spin states and becomes critical for room temperature implementation of qubits, such as quantum sensors in biological systems.

Several design strategies have been explored for tuning the spin relaxation and spin decoherence rates in transition metal complexes. Spin coherence times can be improved by reducing interactions with nuclear spins through ligand substitutions [10], especially when using nuclear-spin-free ligands [11]. Often, the bottleneck of spin coherence times arises from fast spin relaxation, which necessarily destroys coherent states in the transverse plane of the Bloch sphere. Slow spin relaxation is achieved in square-planar or square-pyramidal transition metal complexes, where the spin-orbit coupling becomes quenched by the ligand field [1, 6, 12], minimizing spin-phonon coupling. Systems with a single unpaired electron (S=1/2), such as Cu(II) or V(IV), generally yield slow spin relaxation due to the absence of Orbach relaxation involving low-lying electronic excited states. However, a better understanding of structural effects on spin-lattice relaxation is crucial for mitigating molecular qubit decoherence at room temperature.

Hadt and co-workers have previously developed a ligand-field model to describe the couplings between optical modes and the M_s sublevels of S=1/2 systems [6, 12, 13]. From the development of a group theoretical selection rule, it was determined that only symmetric (bond-stretching) modes are fully allowed to undergo linear spin-phonon couplings. This selection rule derives from the fact that ligand field excited states distort along totally symmetric modes. These vibronic couplings change the degree of spin-orbit coupling between the ground and excited states, which can modulate groundstate orbital angular momentum and minority spin contributions in the ground-state wavefunction, thus leading to spin relaxation. Notably, changes in molecular symmetry will also lead to changes in vibrational symmetries, including the number of totally symmetric irreducible representations [6, 14]. Furthermore, ligand perturbations can also change the energies of acoustic and optical modes and, therefore, their thermal population. Indeed, systematic correlations between molecular structure, vibrational mode symmetries, and spin relaxation have provided invaluable mechanistic insight related to the magnitude of T_1 and its temperature dependence.

Nemykin and co-workers have recently presented a detailed spectroscopic study of a new vanadyl complex related to VOPc: vanadyl tetrapyrazinoporphyrazine with eight peripheral 2,6-diisopropylphenol groups (VOPyzPz-DIPP, Fig. 1b). Here, we quantify the spinlattice relaxation time, T_1 , of VOPyzPz-DIPP in solid

state dilutions, as well as its T_1 orientation dependence at $100 \,\mathrm{K}$. VOPyzPz-DIPP exhibits room temperature coherence with a T_1 comparable to VOPc. It also exhibits a slightly longer T_1 at 5 K despite the peripheral groups that introduce additional phonon modes. There exists, however, a dramatic difference in the T_1 temperature dependence between the two vanadyl complexes, especially in the intermediate temperature range (10–100 K) where VOPyzPz-DIPP relaxes more rapidly than VOPc. This relaxation behavior is tentatively assigned to increased spin-phonon couplings between the spin and new lowenergy vibrational degrees of freedom introduced by the PyzPz-DIPP ligand. Thus, this study provides new insights into the spin-phonon coupling contributions to T_1 over a large temperature regime.

MATERIALS AND METHODS

Materials

VOPc and titanyl phthalocyanine (TiOPc) were purchased from Sigma-Aldrich. VOPc was diluted by the isostructural diamagnetic TiOPc in a ratio of 1:100 as described in a previous study [4], resulting in a bright primary-blue polycrystalline powder. VOPyzPz-DIPP was prepared as described previously [15]. As shown in Fig. 1, VOPyzPz-DIPP has an analogous structure to VOPc. A 3D interactive rendering of the VOPyzPz-DIPP molecule is available from the CCDC database (ref no. 2208789). For EPR measurements, VOPyzPz-DIPP was also diluted

Fig. 1. Molecular structures of (a) VOPc and (b) VOPyzPz-DIPP.

by its diamagnetic titanyl counterpart, TiOPyzPz-DIPP, in a ratio of 1:100. The resulting material is a deep dark green powder (photos of the materials and the UV-vis spectrum of VOpyzPz-DIPP are included in the SI). The color hues used to visualize the data in Figs. 2–4 represent the colors of the actual materials (with tints and shades adjusted for clarity). The X-ray powder diffraction of VOPyzPz-DIPP (Fig. S19) shows contributions from a crystalline structure on top of broad amorphous-like peaks. The crystal unit cell for VOPyzPz-DIPP is large, with a cubic lattice parameter of 37.267 Å, which may lead to a partial loss of long-range order in the EPR diamagnetic dilution.

Electron Paramagnetic Resonance (EPR)

Continuous wave (CW) EPR was performed at X-band by a Bruker EMX instrument at 77 K using a liquid nitrogen immersion dewar. CW spectra were fitted using EasySpin [16] to extract *g* values and hyperfine parameters (Figs. S3–S4).

Pulse EPR enables the measurement of the spin relaxation dynamics. Pulse X-band EPR experiments were

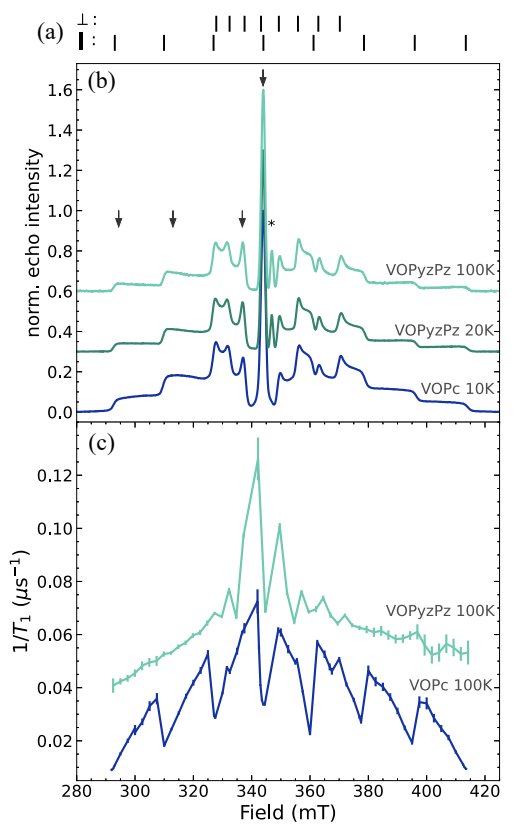


Fig. 2. (a) Simulated orientation dependence of VOPc, showing where parallel and perpendicular orientations of the molecular principal axis with respect to the external field are probed. (b) EDFS of VOPyzPz-DIPP (20 K and 100 K) and VOPc (10 K) [5]. Arrows indicate field positions selected for temperature-dependent T_1 measurements. Asterisk denotes the feature resulting from an organic radical in the TiO matrix. (c) Spin-lattice relaxation time T_1 at 100 K as a function of the external magnetic field measured by inversion recovery experiments. Error bars show the 95% confidence interval of the fits using Eq. 2.

conducted with a Bruker ELEXSYS E580 pulse EPR spectrometer, using a Bruker MD-4 resonator. Temperature control was achieved with an Oxford Instruments CF935 cryogen flow cryostat using liquid helium and a Mercury iTC temperature controller. By selecting different high-power microwave pulse sequences, both T_1 and $T_{\rm m}$ can be measured. Due to spin-spin interactions, spins in different environments process at slightly different frequencies causing phase decoherence (T_m) . This was probed using Hahn-echo pulse sequences, $\pi/2 - \tau - \pi$ τ – echo, by increasing τ and observing the decrease in the integrated echo intensity. Echo-detected field sweep (EDFS) spectra employed the same two-pulse Hahoecho sequence while scanning through different magnetic fields. Thermal equilibration through spin-lattice relaxation (T_1) , realigns the spins back with the external magnetic field. This relaxation was detected by inversion recovery experiments, which added an initial spin flip π pulse to the sequence: $\pi - t - \pi/2 - \tau - \pi - \tau$ – echo (τ is a fixed constant and t is the variable time delay).

Besides measuring T_1 , inversion recovery traces may also contain relaxation by spectral diffusion, where excited spins exchange energy with spins outside of the microwave pulse bandwidth [17]. This additional (fast) relaxation pathway becomes particularly prominent at low temperatures when the spin lifetimes are long. To isolate this effect from the actual spin-lattice relaxation, saturation recovery measurements were also performed (see Section S3.2). This technique implements a series of eight initial π pulses, saturating spectral diffusion and diminishing its contributions to the subsequent inversion recovery measurements.

RESULTS AND DISCUSSION

Hahn-echo measurements of $T_{\rm m}$ at X-band show a stretch exponential decay of the echo intensity convoluted by hyperfine modulations (Figs. S15–S17). The modulations arise from interactions with coupled nuclear spins on ligand atoms (H and N) and inhibit a quantitative determination of $T_{\rm m}$. Nonetheless, as shown qualitatively in Fig. S18, the phase-memory time seems larger for VOPyzPz-DIPP than for VOPc. This validates the strategy of adding bulky ligand substituents to improve spin coherence by increasing the distance between spin centers as proposed in [15]. Additional experiments are required for a detailed analysis of $T_{\rm m}$; we focus here on the spin-lattice behavior, $T_{\rm l}$.

The EDFSs for VOPc and VOPyzPz-DIPP are similar (Fig. 2b), reflecting comparable spin Hamiltonian parameters and first coordination spheres. The *g* values and hyperfine parameters extracted from CW EPR measurements are presented in Table S1 and agree well with previous studies [3–5]. The spectrum of VOPyzPz-DIPP has an additional feature (marked by an asterisk) attributable to an organic radical with a *g* value of 2.003. CW EPR shows that it stems from the TiOPyzPz matrix (Fig. S6).

This feature is also captured by CW EPR in VOPc, per previous studies [3, 4]. The presence of such a radical signal, however, does not affect the measurement of T_1 at other field positions.

 T_1 was measured by inversion recovery and as a function of the external field at 100 K (Fig. 2c). The relaxation is anisotropic and becomes monotonically faster towards the center of the spectrum. Vanadyl porphyrins and phthalocyanines possess axial g- and A-tensors with $g_{\parallel} < g_{\perp}$ and $|A_{\parallel}| < |A_{\perp}|$, where parallel and perpendicular refer to the orientation of the external field with respect to g_z (the z-axis is approximately collinear with the principal symmetry axis, out of the equatorial plane in Fig. 1). Since the perpendicular and parallel spin Hamiltonian parameters are distinct, different field positions measure different orientations and single crystals are not required to measure T_1 anisotropy. Calculations of the hyperfine splitting of VOPc with the I=7/2 ⁵¹V nucleus show the field positions of parallel and perpendicular orientations in Fig. 2a [5]. We probe pure parallel contributions at 294 mT, while the isolated contribution of perpendicular orientations is measured at 337 mT (see arrows in Fig. 2b). T_1 is longest at the parallel position and decreases linearly through intermediate orientations towards the perpendicular orientation.

VOPc and several other molecular qubits show similar relaxation behavior [5]. In agreement with previous measurements, VOPc exhibits sharp discontinuities at the hyperfine turning points (i.e. steps and peaks of the EDFS spectrum, blue curve in Fig. 2c). These discontinuities arise due to the excitation of new M_1 subpopulations with different rates of spin relaxation. Notably, the relaxation of VOPyzPz-DIPP is insensitive to the hyperfine turning points. A possible origin of this effect lies in the partially amorphous nature of the material as measured by XRD (Fig. S19). The local behavior around the V(IV) spin center seems unaffected, as seen by the sharp turning points of the EDFS spectra, but long-range structural disorder would affect the propagation of phonon modes at low energies. Structural symmetries might become lifted, allowing long wavelength glassy phonons to partake in the relaxation and cause a blurring of the hyperfine turning points. Future research directions include quantifying such an effect of structural disorder on spin-lattice relaxation.

The anisotropy parameter for VOPyzPz-DIPP can be computed by taking the ratio of T_1 at the parallel and perpendicular field positions (Eq. 1):

$$T_{1,\text{anisotropy}} = \frac{1/T_1(\perp)}{1/T_1(||)} = 2.2.$$
 (1)

The T_1 anisotropy of 2.2 is close to the average predicted value of 2.5 from explicit forms of the spin-orbit wave functions [5]. Interestingly, the T_1 anisotropy of VOPc deviated significantly from 2.5 in a previous study, exhibiting a value of 6.0. This deviation from 2.5 was attributed to the square pyramidal geometry of VOPc,

which breaks the planar symmetry and allows for additional modes to undergo spin-phonon and vibronic couplings. These additional relaxation pathways can result in a deviation from the average value of 2.5. Since both VOPc and VOPyzPz-DIPP have the same local symmetry around the vanadyl center, the different T_1 anisotropies suggest that additional long-range phonon modes may play an important role in the spin-lattice relaxation of VOPyzPz-DIPP. Such modes could arise from low energy vibrations of the peripheral groups and from glassy modes of the amorphous structure.

To further explore the vibrational contributions to the T_1 of VOPyzPz-DIPP, we performed inversion recovery measurements on VOPyzPz-DIPP and VOPc between 5 K and room temperature (Figs. 3 and 4). Data for VOPc are consistent with previous studies [3, 4]. Temperature-dependent T_1 was measured at various field positions (arrows in Fig. 2a). All fields exhibited similar temperature behavior; thus, we focus on the powder line (i.e. the field position with the strongest signal intensity at 343 mT), while data for other field positions are presented in Section S3.2.

Inversion recovery quantifies the intensity of the echo measured at different delay times after the inversion π pulse. As shown in Fig. 3a, the polarization of the spins (sign of the echo intensity) relaxes back to equilibrium with increasing delays. At 10 K (Fig. 3a), VOPyzPz-DIPP relaxes faster than VOPc. T_1 can be obtained by fitting the data to Eq. 2,

$$I(t) = A \exp\left(\left(\frac{t}{T_1}\right)^{\beta}\right) + I_0.$$
 (2)

where β is a stretching factor that describes the deviation from a pure exponential decay. As seen from the smaller fit residuals in Fig. 3b, the relaxation of VOPyzPz-DIPP

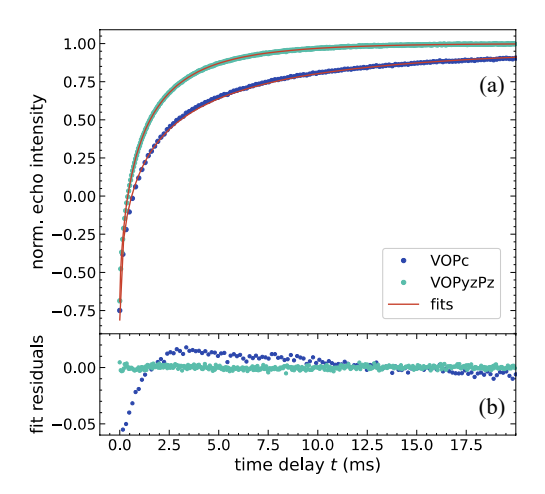


Fig. 3. Spin lattice relaxation measured by inversion recovery at 10 K. (a) Normalized integrated echo intensity of VOPyzPz and VOPc (markers) with stretch exponential fits (solid lines). (b) Fitting residuals corresponding to fits of panel a.

is better expressed by such a stretched exponential over the entire time interval, as compared to the relaxation of VOPc. Values of β are also closer to unity for VOPyzPz-DIPP at low temperatures (Figs. S12–S13), indicating that it follows a simpler decay process. This simpler decay is a desirable feature for implementing qubits into real devices as it improves their controllability [10]. For VOPc, we attempted biexponential fits that have been proposed to separate the slow spin-lattice relaxation from a fast spectral diffusion. Such fits (that omit β), however, gave even larger residuals. We therefore moved to collect measurements of T_1 by saturation recovery, particularly at low temperatures where relaxation is slower and more affected by spectral diffusion. As shown in Fig. S14, saturation recovery indeed measures slower spin-lattice relaxations. It captures, however, the same temperature dependence of T_1 as the inversion recovery measurements presented here. The spectral diffusion measurements, therefore, validate the time constants obtained from fitting VOPc T_1 data with stretched exponential functions, despite the larger residuals obtained.

Figure 4a shows $1/T_1$ measured by inversion recovery at the powder line (344 mT) as a function of temperature. Our experiments reproduce the behavior of VOPc reported previously [4], showing two different

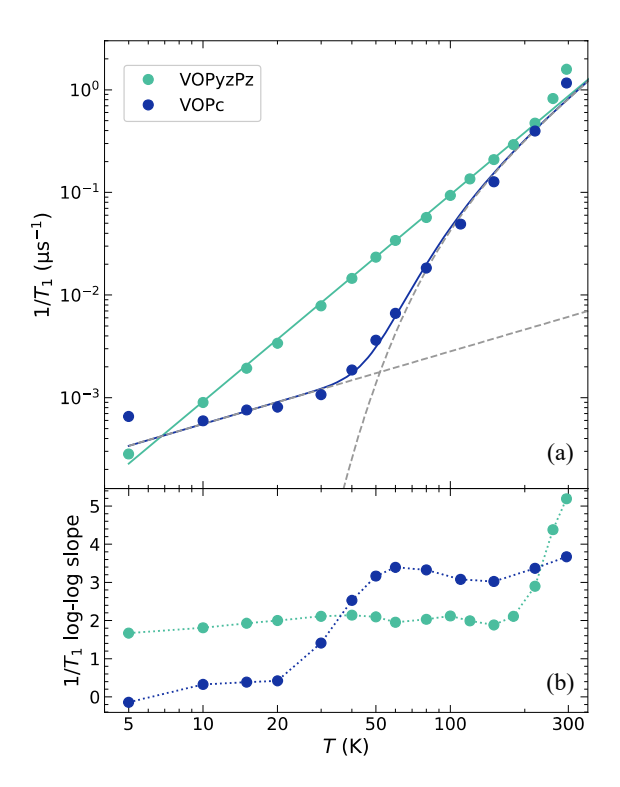


Fig. 4. Spin-lattice relaxation of VOPyzPz-DIPP and VOPc as a function of temperature collected by inversion recovery at the powder line (344 mT). (a) Experimental $1/T_1$ data (markers) fitted by Eq. 4 as described in the text (solid lines). Dashed lines show individual contributions to the fit from a power law and local modes in VOPc. Fitting errors are smaller than the marker sizes. (b) Slope of $1/T_1$ computed in a log-log scale, revealing changes in the temperature dependence of T_1 .

temperature regimes depicted by the dashed lines. This change in slope (plotted in Fig. 4b) indicates that different relaxation processes are active at these different temperature ranges. Other porphyrin-based qubits show an analogous temperature dependence with a change of slope around 40-60 K [14]. The behavior of VOPyzPz-DIPP is surprising, following a simple power law (solid green line) with no clear switch in the relaxation mechanism with temperature. Its spin-lattice relaxation time is faster than VOPc for most of the temperature range. reaching approximately the same values at room temperature. At 5 K, however, T_1 appears longer for VOPyzPz-DIPP, which is corroborated by the saturation recovery measurements (see Fig. S14). At temperatures above 5 K, vibrational modes become more populated. Adding the peripheral groups to the molecule raises the number of available modes, particularly of low-energy phonons that are more accessible at low temperatures. The partial amorphous nature of the lattice could also add low energy vibrations enhancing this effect further. This enhanced phonon population could explain the steeper slope of T_1 of VOPyzPy-DIPP at low temperatures compared to VOPc.

Spin-lattice coupling reflects the dependency of electronic states on deformations of the lattice due to vibrations. This dependency follows different mechanisms for different phonon energies. At very low temperatures, the energy of the phonons is of the same magnitude as the Zeeman splitting, allowing a *direct* excitation or absorption of phonons by spins. The probability of such a relaxation scales linearly with temperature [18] and typically involves acoustic phonons with large wavelengths that cause minimal molecular distortions. At temperatures below 4K, deviations from this linear behavior caused by phonon bottleneck effects have been reported for CuPc [19].

When two phonons become involved in a *Raman* spin relaxation event, higher energy vibrational modes can participate, as only the difference in their energy must match the spin-flip transition energy. Starting from a second-order spin-phonon Hamiltonian, a two-phonon Green's function formalism predicts an exponential temperature dependence for such a two-phonon spin scattering ($\propto e^{E_{loc}/k_BT}$) [20]. Given the functional form, this process becomes particularly important at higher temperatures where optical phonon modes dominate. On the other hand, the low-energy (acoustic) phonon behavior of crystals is often described using a Debye model (where the phonon density of states follows a quadratic energy dependence up to a Debye temperature θ_D , at which all modes have become thermally accessible). Applying the Debye model to the same spin-phonon Hamiltonian gives a power-law temperature dependence for the spin relaxation ($\propto T^n$) [21]. In the low-temperature limit $(\theta_{\rm D} >> T)$ an exponent of n=7 is obtained (which has been a traditional assumption [18, 22]), but n is usually smaller for molecular crystals, reaching a value of 2 in

the high-temperature limit ($\theta_D \ll T$) [21]. All contributions are summarized in Eq. 3 [4]:

$$\frac{1}{T_1} = a_{\text{dir}}T + a_{1,\text{Ram}} \left(\frac{T}{\theta_D}\right)^n + a_{2,\text{Ram}} \frac{e^{E_{\text{loc}}/k_B T}}{(e^{E_{\text{loc}}/k_B T} - 1)^2}$$
(3)

$$\frac{1}{T_1} \approx a \ T^n + b \frac{e^{E_{\text{loc}}/k_B T}}{(e^{E_{\text{loc}}/k_B T} - 1)^2}$$
 (4)

Since the direct process is prevalent only near liquid helium temperatures, we avoid overfitting by combining the direct and Debye-Raman terms (Eq. 4) as previously proposed [14].

As shown in Fig. 4a, the relaxation of VOPc is wellfitted by Eq. 4. It follows power-law behavior at low temperatures (n=0.7, straight dashed line in Fig. 4a), while local modes around $E_{loc} = 233 \, \text{cm}^{-1}$ dominate the relaxation above 50 K (in a previous study that included all terms of Eq. 3, the local mode energy was fitted to 295 cm⁻¹ [4]). The data point at 5 K was not included in the fit, because it deviates from the T_1 behavior measured by saturation recovery (see Fig. S13). However, fits to the saturation recovery measurements that include data at 5 K result in a similar exponent of n=0.6. Such a low power law exponent suggests that relaxation involving two phonons is limited and that the direct mechanism dominates at these temperatures. The energy of the local mode that controls the high-temperature behavior falls within the energy range of totally symmetric modes containing the metal-ligand bond-stretching character, which is consistent with our previous ligand field model for VOPc [6]. The behavior of VOPc is hence dictated by strong coupled optical modes around 233 cm⁻¹ at elevated temperatures (> 50 K), while two-phonon processes are inefficient below 40 K, resulting in a spin-lattice relaxation that increases only weakly with temperature.

The relaxation of VOPyzPz-DIPP follows a single power law behavior from 5K up to room temperature with n=2.0. There is no single mode that dominates any part of the spectrum, but rather an unresolved collection of acoustic and optical phonon modes. VOPyzPz-DIPP reaches the same value of T_1 as VOPc, however, suggesting that a local mode at similar energies may play an important role at room temperature. Interestingly, a power-law exponent of 2 is predicted in the high-temperature limit of a Debye model ($\theta_D \ll T$) [21]. This implies that VOPyzPz-DIPP has a low Debye temperature where vibrational modes that contribute to a Raman relaxation are populated already at low temperatures. We note that a Debye model is not required to reach this result. By assuming that the phonon modes are well populated, $E_{\rm ph}$ << T, the exponential local mode expression (last term in Eq. 4) can be expanded into a Taylor series with a leading term that also scales as T^2 . This can be visualized in Fig. 4a where the exponential term (blue curve) reaches the same asymptote as the power law fit with n=2 (green

curve) beyond room temperature. Notably for VOPyzPz-DIPP, this high-temperature limit extends down to low temperatures, indicating that low-energy phonons are essential to its relaxation. As discussed above, VOPyzPz-DIPP is indeed expected to have more of such low-energy modes than VOPc. Additionally, the peripheral groups of VOPyzPz-DIPP break the planar symmetry of the ligand, which according to our ligand-field model [6, 12, 13], could loosen the selection rules and allow additional modes to couple more efficiently with spins. Thus, an abundance of low-energy phonons and additional coupling pathways would explain the T_1 behavior of VOPyzPz-DIPP.

Further experiments to measure the phonon spectrum are necessary to confirm these results. Due to their accessibility via Raman, IR, and THz spectroscopy, highenergy optical mode contributions to spin relaxation are currently best understood. For many molecular qubit candidates, including VOPc, specific optical modes couple strongest with spins and play the dominant role in spin relaxation. We demonstrated here that understanding the low-energy phonon behavior can also be important, particularly when studying the low-temperature behavior and structural dependencies of spin relaxation mechanisms. This contribution calls for experimental techniques such as inelastic neutron and X-ray scattering that can transfer momentum to the material and excite all phonon modes. To date, only two such studies have been published. They show how low-lying optical modes are critical for spin relaxation [23], and that phonon modes themselves can be coupled, which transfers the strong spin-lattice coupling from optical to highly populated acoustic modes [24].

CONCLUSIONS

Using pulse EPR techniques, we compared the spinlattice relaxation behaviors of VOPyzPz-DIPP and VOPc. At 5 K, VOPyzPz-DIPP appears to have a slower T_1 than VOPc. Both follow a power law temperature dependence at low temperatures, but VOPyzPz-DIPP has an exponent that is 2.8 times larger than VOPc. This difference suggests that VOPyzPz-DIPP has more lowenergy phonon modes that are available for spin-lattice relaxation, resulting in shorter spin-lattice relaxation beyond 10 K. In contrast to VOPc, where T_1 has two temperature regimes with distinct decay mechanisms, the T_1 behavior VOPyzPz-DIPP is governed by the same power law up to room temperature. A picture where a single local phonon mode dominates the spin-phonon coupling at elevated temperatures, therefore, cannot explain the T_1 behavior of VOPyzPz-DIPP. For VOPyzPz-DIPP, spin relaxation is likely the result of coupling with several acoustic and optical modes that may become available due to symmetry breaking, as well as additional phonon modes from the peripheral groups and structural disorder. This abundance of phonon modes available for spin-lattice coupling would also explain the differences in T_1 anisotropy for the two compounds (VOPyzPz-DIPP=2.2 and VOPc=6.0).

Acknowledgments

We acknowledge Paul H. Oyala for his support with the pulse EPR measurements. N.P.K. acknowledges support from the Hertz Fellowship. N.P.K. and K.M.L. both acknowledge support from the National Science Foundation Graduate Research Fellowship Program under Grant No. DGE-1745301. Generous support from the NSF (CHE-2153081), Minnesota Supercomputing Institute, and the University of Tennessee to V.N. is greatly appreciated. Financial support from the Research Corporation for Science Advancement (RCSA) through a Cottrell Award (Award ID: 28165) is gratefully acknowledged (R.G.H.).

Supporting information

Additional data are given in the supplementary material. This material is available free of charge *via* the Internet at http://www.worldscientific.com/doi/suppl/10.1142/S1088424624500329

Crystallographic data have been deposited at the Cambridge Crystallographic Data Centre (CCDC) under the numbers CCDC-2208789. Copies can be obtained on request, free of charge, *via* https://www.ccdc.cam.ac.uk/structures/ or from the Cambridge Crystallographic Data Centre, 12 Union Road, Cambridge CB2 1EZ, UK (fax: +44 1223-336-033 or email: deposit@ccdc.cam.ac.uk)

REFERENCES

- Atzori M and Sessoli R. J. Am. Chem. Soc. 2019; 141: 11339–11352.
- 2. DiVincenzo DP and IBM. *Fortschr. Phys.* 2000; **48**: 771–783.
- 3. Atzori M, Tesi L, Morra E, Chiesa M, Sorace L and Sessoli R. *J. Am. Chem. Soc.* 2016; **138**: 2154–2157.
- 4. Follmer AH, Ribson RD, Oyala PH, Chen GY and Hadt RG. J. Phys. Chem. A 2020; 124: 9252–9260.
- Kazmierczak NP and Hadt RG. J. Am. Chem. Soc. 2022; 144: 20804–20814.

- 6. Kazmierczak NP, Mirzoyan R and Hadt RG. *J. Am. Chem. Soc.* 2021; **143**: 17305–17315.
- Warner M, Din S, Tupitsyn IS, Morley GW, Stoneham AM, Gardener JA, Wu Z, Fisher AJ, Heutz S, Kay CWM and Aeppli G. *Nature* 2013; 503: 504–508.
- Bonizzoni C, Ghirri A, Atzori M, Sorace L, Sessoli R and Affronte M. Sci. Rep. 2017; 7: 13096.
- Cimatti I, Bondì L, Serrano G, Malavolti L, Cortigiani B, Velez-Fort E, Betto D, Ouerghi A, Brookes NB, Loth S, Mannini M, Totti F and Sessoli R. Nanoscale Horiz. 2019; 4: 1202–1210.
- Bader K, Winkler M and Van Slageren J. Chem. Commun. 2016; 52: 3623–3626.
- 11. Zadrozny JM, Niklas J, Poluektov OG and Freedman DE. *J. Am. Chem. Soc.* 2014; **136**: 15841–15844.
- 12. Mirzoyan R, Kazmierczak NP and Hadt RG. *Chemistry A European J.* 2021; **27**: 9482–9494.
- 13. Mirzoyan R and Hadt RG. *Physical Chemistry Chemical Physics* 2020; **22**: 11249.
- Kazmierczak NP, Lopez NE, Luedecke KM and Hadt RG. Chem. Sci. 2024; 15: 2380–2390.
- 15. Marx B, Schrage BR, Ziegler CJ and Nemykin VN. J. Porphyrins Phthalocyanines 2023; 27: 363–372.
- 16. Stoll S and Schweiger A. *Journal of Magnetic Resonance* 2006; **178**: 42–55.
- Eaton SS and Eaton GR. In Harris RK, Wasylishen RL, eds. eMagRes. Chichester, UK: John Wiley & Sons, Ltd, 2016; 1543–1556.
- Standley KJ and Vaughan RA. Electron Spin Relaxation Phenomena in Solids, Boston, MA: Springer US; 1969.
- Standley KJ and Wright JK. *Proc. Phys. Soc.* 1964;
 83: 361–367.
- 20. Gu L and Wu R. Phys. Rev. Lett. 2020; 125: 117203.
- 21. Gu L and Wu R. Phys. Rev. B 2021; 103: 014401.
- Shrivastava KN. *Physica Status Solidi (b)* 1983;
 117: 437–458.
- Garlatti E, Albino A, Chicco S, Nguyen VHA, Santanni F, Paolasini L, Mazzoli C, Caciuffo R, Totti F, Santini P, Sessoli R, Lunghi A and Carretta S. *Nat. Commun.* 2023; 14: 1653.
- Garlatti E, Tesi L, Lunghi A, Atzori M, Voneshen DJ, Santini P, Sanvito S, Guidi T, Sessoli R and Carretta S. *Nat. Commun.* 2020; 11: 1751.